Numerical Study On The Internal Irreversible Flow Loss of Single Screw Expanders

Lili Shen (sll101996@icloud.com)
Beijing University of Technology https://orcid.org/0000-0003-0621-0060
Yuting Wu
Beijing University of Technology
Wei Wang
Beijing University of Technology
Biao Lei
Beijing University of Technology
Wei Duan
Beijing Zhenxing Institute of Metrology and Measurement
Ruiping Zhi
Beijing University of Technology

Original Article

Keywords: Single screw expander, CFD, Mesh deformation approach, Entropy production ratio, Irreversible flow loss

Posted Date: September 20th, 2021

DOI: https://doi.org/10.21203/rs.3.rs-871637/v1

Title page

Numerical Study on the Internal Irreversible Flow Loss of Single Screw Expanders

Lili Shen, born in 1991, is currently a PhD candidate at *Key Laboratory of Enhanced Heat Transfer and Energy Conservation, Ministry of Education and Key Laboratory of Heat Transfer and Energy Conversion, Beijing University of Technology, China*. She received her Ph.D from *Beijing University of Technology, China*, in 2020. Her research interests include computational fluid dynamics and fluid machinery.
E-mail: sll101996@icloud.com, 1019962588@qq.com

Yuting Wu, born in 1970, is currently a professor at *Key Laboratory of Enhanced Heat Transfer and Energy Conservation, Ministry of Education and Key Laboratory of Heat Transfer and Energy Conversion, Beijing University of Technology, China*. His research interests include heat transfer and storage, low-grade energy thermal power conversion and solar thermal power generation technology.
E-mail: wuyuting1970@126.com

Wei Wang, born in 1978, is currently an associate professor at *Key Laboratory of Enhanced Heat Transfer and Energy Conservation, Ministry of Education and Key Laboratory of Heat Transfer and Energy Conversion, Beijing University of Technology, China*. His research interests include renewable energy utilization and building energy conservation.
E-mail: wang_wei@bjut.edu.cn

Biao Lei, born in 1984, is currently an associate professor at *Key Laboratory of Enhanced Heat Transfer and Energy Conservation, Ministry of Education and Key Laboratory of Heat Transfer and Energy Conversion, Beijing University of Technology, China*. His research interests include efficient recycling of industrial waste energy, advanced compressor, heat pump and refrigeration technology.
E-mail: leibiao4151@163.com

Wei Duan, born in 1990, is currently an engineer at *Beijing Zhenxing Institute of Metrology and Measurement, China*.
E-mail: 869178590@qq.com

Ruiping Zhi, born in 1986, is currently an instructor at *Key Laboratory of Enhanced Heat Transfer and Energy Conservation, Ministry of Education and Key Laboratory of Heat Transfer and Energy Conversion, Beijing University of Technology, China*. Her research interests include structural design and optimization of single screw machines.
E-mail: zhiruiping@emails.bjut.edu.cn

Corresponding author：Lili Shen　E-mail：sll101996@icloud.com

ORIGINAL ARTICLE

Numerical Study on the Internal Irreversible Flow Loss of Single Screw Expanders

Lili Shen[1], Yuting Wu[1], Wei Wang[1], Biao Lei[1], Wei Duan[2] and Ruiping Zhi[1]

Received June xx, 202x; revised February xx, 201x; accepted March xx, 202x

Abstract: As a type of positive displacement expander, single screw expander (SSEs) can be widely applied in the energy storage systems and waste heat recovery field. The irreversible losses (such as leakage, flow, heat transfer, intake and exhaust pressure loss…) have great influence on the expander performance. However, irreversible flow loss in the expander is nearly impossible to investigate experimentally and theoretically. In this paper, a three-dimensional computational fluid dynamics (CFD) study of SSE using mesh deformation approach was presented. The CFD model was validated by the experimental results. Field distribution of pressure, temperature and velocity of SSE were carried out. An energy loss factor based on entropy production principle was used to measure the irreversible flow (including leakage) loss. The energy loss caused by direct dissipation and turbulent fluctuation dissipation was compared. The energy loss of different region was investigated. Results show that energy loss of the turbulent dissipation is far more than that of direct dissipation. The energy loss factor decreases from 0.547 to 0.221 when the rotation speed changes from 2000rpm to 4000rpm. The shaft efficiency increases from 39.8% to 52.1% with the internal volume ratio from 3 to 5.

Keywords: Single screw expander • CFD • Mesh deformation approach • Entropy production ratio • Irreversible flow loss

1 Introduction

In recent years, energy and environmental problems are becoming increasingly serious, and technology for renewable energy and waste heat recovery has received more and more attention. As the equipment of energy conversion between thermal energy and mechanical energy, expanders can be widely applied in the energy storage systems and waste heat recovery field. And positive displacement expanders are more suitable for small-scale energy recycle and energy storage systems [1]. As a type of positive displacement expander, SSE can be widely used as being competitive advantages in terms of small capacity, low noise, low vibrations, high volumetric efficiency, smooth operation and long working life [2,3]. However, irreversible losses (like leakage, flow, heat transfer, friction, intake pressure loss, etc.) have great influence on the performance of expanders.

Recent experimental studies on the SSE have been carried out based on the small-scale organic Rankine cycle system [4-8] and compressed air experimental system [9-11], the vast majority of which was analysis on the performance under different working conditions. Wang et al. [12] investigated the effect of the pressure loss in the inlet and exhaust passages on the performance of SSEs. Theoretically, the performance of SSEs mainly has been solved by thermodynamic and semi-empirical models. The semi-empirical model is composed of mass, energy and momentum conservations, but some critical parameters are original from experimental data. Lemort et al. [13] presented the semi-empirical model formerly proposed by Winandy et al. [14] for an open-drive scroll expander. Ziviani et al. [15] developed the semi-empirical model to investigate the performance of SSE affected by internal losses (typically leakage, heat transfer and mechanical losses). Giuffrida et al [5] revised the semi-empirical approach by proposing more physically sound formulations for mechanical losses and ambient heat losses,

✉ Lili Shen
sll101996@icloud.com

[1] Key Laboratory of Enhanced Heat Transfer and Energy Conservation, Ministry of Education and Key Laboratory of Heat Transfer and Energy Conversion, Beijing Municipality, Beijing University of Technology, Beijing 100124, China

[2] Beijing Zhenxing Institute of Metrology and Measurement, Beijing 100074, China

which achieved better accuracy than that of Ziviani et al. [15]. The zero-dimensional thermodynamic chamber model is a theoretical model based on the mass and energy conservations, which is widely used in rotary positive-displacement compressors and expanders for decades [16-20]. For single screw machines, Wang et al. [20] established a thermodynamic model to predict the performance of single screw refrigeration compressor with multicolumn envelope meshing pair. Shen et al. [21] built a thermodynamic model to examine the internal leakage of SSEs. Wu et al. [22] and Guo et al. [23] presented a new method for calculating friction power integrated into the thermodynamic model and analyzed the intake and exhaust structure of the SSE. Wang et al. [24] investigated the characteristics of heat transfer loss of SSE.

Although much attention has been paid to the SSE, the irreversible flow loss of SSE has not been studied yet. Recently the computational fluid dynamics (CFD) as a way of calculating three-dimensional flow field have been broadly applied to estimating dynamic flow characteristics in the positive displacement type compressors and expanders. However, CFD studies on single-screw machines are limited. Some of the challenges when performing CFD studies in the SSEs is the complexity of the middle dynamic deformation region caused by the screw rotor and gaterotors motion. Suman et al. [25] and Ziviani et al. [26] evaluated different mesh techniques based on different commercial software both in steady-state and transient conditions to identify the most suitable method to simulate the SSE. Only Chimera strategy could perform the transient simulation in their study. Casari et al. [27,28] analyzed the applicability of OpenFOAM with CFD simulations of SSEs and obtained the temperature distribution of screw rotors. Shen et al. [29] studied the periodic curve of pressure and velocity of three monitor points in the SSE using dynamic deformation mesh. Casari et al. [30] investigated dynamic flow characteristics in the SSE with the use of the chimera strategy. In order to predict internal irreversible flow loss in the SSEs, further research is necessary.

In this paper, a three-dimensional CFD model of SSE was presented. According to the CFD simulation, internal flow field distribution in the SSE was predicted. An energy loss factor based on entropy production principle was proposed to measure the irreversible flow (including leakage) loss. The energy loss caused by viscous dissipation and turbulent dissipation have been analyzed. And the energy flow loss of inlet, middle rotors and outlet region have been compared. Energy loss factor and shaft efficiency under different internal volume ratio and rotation speed have been carried out.

2 CFD model

2.1 Geometry model

SSEs have three main components, namely, screw rotor, gaterotors, and shell. The rotors of SSE are shown in Figure 1. The working chamber is divided into the upper and lower volume by the two symmetrical gaterotors. Therefore, there are two working volume in the SSE during the intake, expansion and discharge working process. In order to facilitate simulation, a three-dimensional CFD geometry model of the single-screw is built, as shown in Figure 2. The CFD region consists three parts: inlet triangle hole, middle rotors domain and outlet region. Three cross sections shown in Figure 2 have been given to make gaps clear. Figure 3 shows the diagram of gaps in the CFD model. In this study, the fitting gaps between the screw rotor and the inner wall of shell are in the range of (80-100) μm (Figure 3a), the meshing gaps between the screw rotor and the gaterotors are in the range of (50-110) μm (Figure 3b), the gaps between the gaterotors tooth surface and the inner wall of shell are about 60μm (Figure 3c).

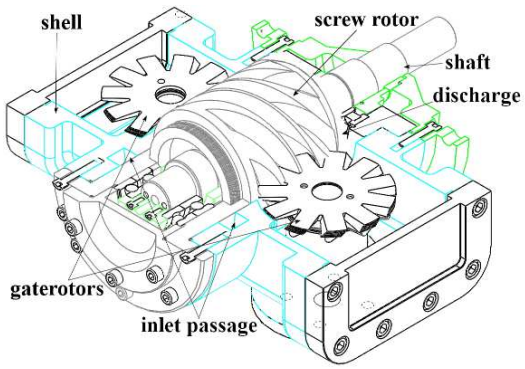

Figure 1 The rotors of the SSE

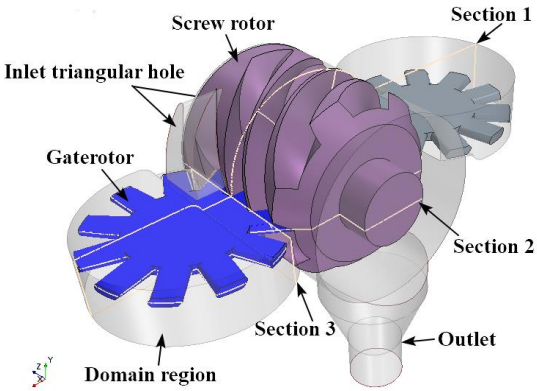

Figure 2 CFD geometry model of the SSE

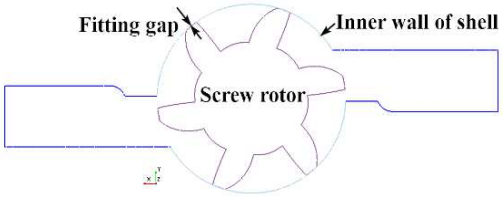

(a). Section 1

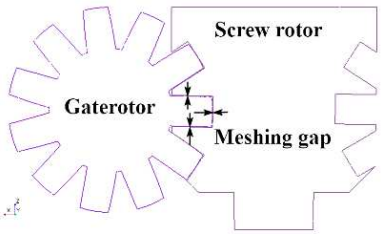

(b). Section 2

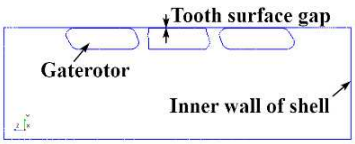

(c). Section 3

Figure 3 Diagram of gaps in the CFD model

2.2 Grid generation

The three-dimensional geometry model of the SSE is decomposed into the inlet, outlet and middle rotors domain. Here, the modeling of deformation and rotation of the middle domain between rotors and shell is the most challenging task. Mesh of the middle domain is created at each time step according to the rotors position. In order to ensure geometry feature and grid quality, the surface mesh of screw rotor and gaterotors are generated based on the same size (i.e. 1mm), as shown in Figure 4. The surface mesh of rotors is generated using ANSA software. Then the volume mesh of middle dynamic domain is generated using the trimmed mesh of STAR-CCM+, which is more suitable for the complex geometry of fluid regions. The stationary domain including the inlet triangle hole and outlet port are provided as separate mesh, and polyhedral mesh is used for the stationary region.

Different regions are connected through fluid-fluid interfaces, where the flux of mass, momentum and energy is conserved, as shown in Figure 5. The progressive meshes were used for fine local refinement at the small clearance and dynamic rotors curved surface, see the inclined section of Figure 5. Due to the rotor rotation, the mesh deformation of dynamic region is of interest. This is realized by using a JAVA macro routine, which can generate new mesh based on initial surface mesh at each time step. But the time step is not given arbitrarily, it mainly depends on the rotation speed, the grooves number of main screw rotor, the grid scale and the solution strategies. In this study, the time step is 2e-3/(z1·n) and its order of magnitude is 1e-6. The rotation angle of each rotation is 0.72º and it takes the screw rotor 500 time-steps during one revolution. The outlet pressure boundary conditions are used at the inlet and outlet. The dynamic boundary is the wall of screw rotor and gaterotors, while the others are assigned no-slip walls as stationary boundary. Besides, all walls are considered to be adiabatic. The total cells number at the beginning of iteration is 2,023,860. The nodes, faces and cells number of each region are given in the Table 1 and the primary structural parameters of the SSE are shown in Table 2.

Mesh generation and CFD software take a lot of computer resources. A server computer with the memory of 32 CPU and the processor of 32 Core was used to obtain the converged solution. The total solver elapsed time is the cumulative time taken to run the entire solution. The average total solver elapsed time is about 218h.

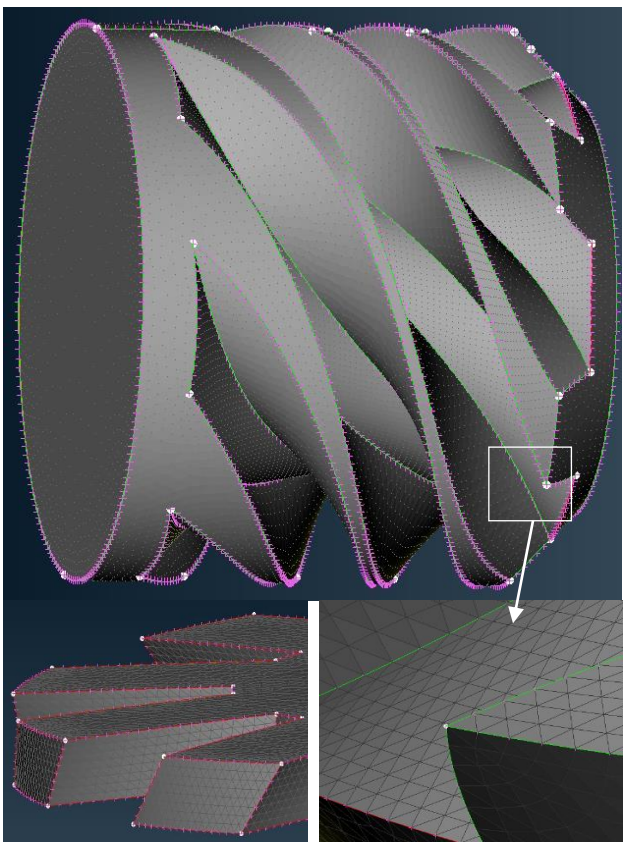

Figure 4 The surface mesh of rotors

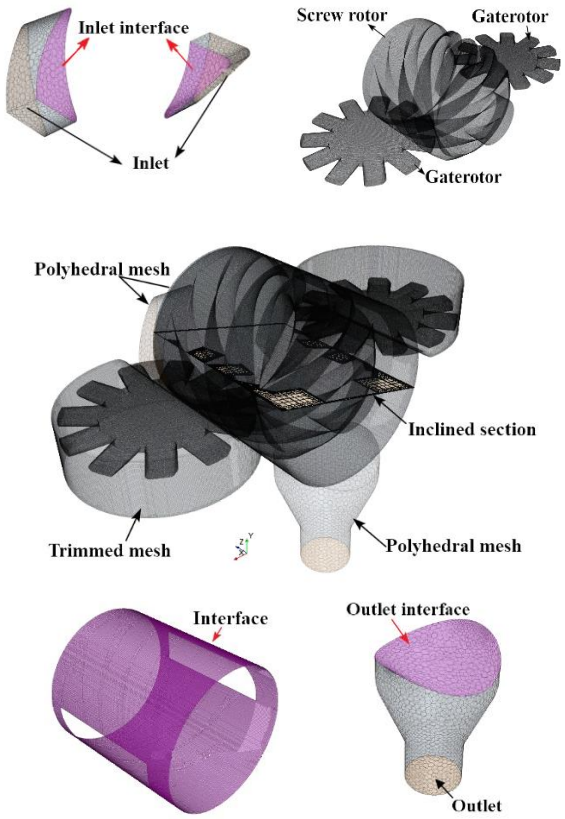

Figure 5 The mesh of working domain of SSE

Table 1 The number of nodes, faces and cells at different region

Type	Inlet region	Working region	Outlet region
nodes	161722	2703104	27338
faces	178968	5747159	29752
cells	27526	1991528	4806

Table 2 Primary structural parameters of SSE

Property	Symbol	Value
Screw lobe	z_1	6
Gaterotor teeth	z_2	11
Screw diameter	d_1	117mm
Gaterotor diameter	d_2	117mm
Center distance	A_c	93.6mm
Gaterotor tooth width width	b	17.1mm

2.3 Mathematical model

The finite volume method can accommodate both structured and unstructured moving grids with cells of arbitrary topologies, and it can be used to discretize fluid flow equations of SSEs. Based on the mass, energy and momentum conservation, the governing equations for the control volume are given in Eq. (1)

$$\frac{\partial}{\partial t}\int_{CV}(\rho\phi)\mathrm{d}V+\int_{A}\boldsymbol{n}\cdot(\rho\boldsymbol{u}\phi)\mathrm{d}A=\int_{A}\boldsymbol{n}\cdot(\Gamma_{\phi}\mathrm{grad}\phi)\mathrm{d}A+\int_{CV}S_{\phi}\mathrm{d}V \quad (1)$$

Where ϕ is the dependent variable, Γ_{ϕ} is diffusion coefficient and S_{ϕ} is source. These four terms describe the effect of time, convection, diffusion and source, respectively. In this study, second-order upwind scheme is used for discretization of convection term and diffusion. Computing gradients are necessary in the governing equation solution methodology. The Hybrid Gauss-least square fitting method is more accurate for cell gradient calculations than the Green-Gauss method. The transient term is discretized through first-order temporal scheme, and the time interval can be divided into an arbitrary number of subinterval time steps. Considering that the working fluid flow in the SSE is compressed air. The equation of state for ideal gas is used. The implicit coupled algorithm is used to solve the non-linear algebra equations. The algebraic multigrid with Bi-conjugate gradient stabilized methods are used to improve the robustness and the speed of convergence.

Three numerical methods including the direct numerical simulation, the large eddy simulation and the Reynolds averaged Navier-Stokes simulation, can be applied to solve the governing differential equations. The former two simulation simulations require the relatively smaller space and time scale to describe the length scale of eddies, which cost much more computer resources than the Reynolds averaged Navier-Stokes simulation. Since the Reynolds averaged Navier-Stokes simulation focus on mean fluid flow characteristics of the complex turbulent flow and it has been widely used in describing the unsteady flow of positive displacement machines. Thus, the Reynolds averaged Navier-Stokes simulation is used to simulate the transient flow of SSE. Two-Equations Realizable k-ε turbulent model was employed, which is suitable for the swirling flow and the flow around a curved screw groove wall in the SSE.

For the convergence criterion, there are two ways to judge it in this study. One is the minimum monitor residual value is less than a specified value according to residual plot, the residuals order-of-magnitude of mass and energy balances is 1e-6 and 1e-4, respectively. The other is to monitor quantities of engineering interest, such as velocity, pressure, torque and mass flow rate changes. These variable parameters within one cycle do not change with the iteration. Take the pressure for example, the difference between the discharge pressure and the last value is less than a certain value, which indicates the simulation has reached steady-state.

2.4 Entropy production rate

According to the Reynolds averaged Navier-Stokes approach, the entropy equation can be divided into time-mean and fluctuating parts [31,32], the equation can be expressed as follows:

$$\frac{\partial(\rho\bar{s})}{\partial t}+\frac{\partial(\rho\bar{u}_i\bar{s})}{\partial x_i}=\overline{\mathrm{div}\left(\frac{\vec{q}}{T}\right)}-\frac{\overline{\partial(\rho u_i's')}}{\partial x_i}+\frac{\overline{\Phi}}{T}+\frac{\overline{\Phi_\Theta}}{T^2} \tag{2}$$

On the right-hand side of two terms $\overline{\Phi}/T$ and $\overline{\Phi_\Theta}/T^2$ are entropy production terms. The first term is entropy production by dissipation including viscous dissipation and turbulent dissipation. The second term describes entropy production by heat transfer. In Ref. [24] the effect of heat transfer on the performance of SSE was relatively small, they are neglected in our CFD simulation. Therefore, the entropy production rate of direct dissipation and turbulent dissipation can be written as:

$$S_{\mathrm{PRO,\bar{D}}}=\frac{\mu}{\bar{T}}\left[2\left(\frac{\partial\bar{u}_i}{\partial x_i}\right)^2+\left(\frac{\partial\bar{u}_i}{\partial x_j}+\frac{\partial\bar{u}_j}{\partial x_i}\right)^2\right] \tag{3}$$

$$S_{\mathrm{PRO,D'}}=\frac{\mu}{\bar{T}}\left[2\overline{\left(\frac{\partial u_i'}{\partial x_i}\right)^2}+\overline{\left(\frac{\partial u_i'}{\partial x_j}+\frac{\partial u_j'}{\partial x_i}\right)^2}\right] \tag{4}$$

Due to the turbulent dissipation rate ε and the mean temperature $\bar{T}$ is included in k-ε turbulent model [33], the Eq.(4) can be given by

$$S_{\mathrm{PRO,D'}}=\frac{\rho\varepsilon}{\bar{T}} \tag{5}$$

Then the entropy production rate can be calculated by the known pressure and temperature field of CFD simulation.

Energy loss caused by entropy production rate is obtained

$$I=\dot{m}S_{\mathrm{PRO}} \tag{6}$$

Power output and shaft efficiency are two important performance reference of SSEs. An energy loss factor ζ is put forward to measure the effect of irreversible flow (including leakage) loss on the power output of SSE, it can be expressed as

$$\eta_{\mathrm{sh}}=\frac{P}{\dot{m}(h_{\mathrm{in}}-h_{\mathrm{d,iso}})} \tag{7}$$

$$\zeta=\frac{I}{(h_{\mathrm{in}}-h_{\mathrm{d,iso}})} \tag{8}$$

Where $\dot{m}$ is the mass flow rate in kg/s, I is Energy loss in kJ/kg, P is power in kW, h_{in}, $h_{\mathrm{d,iso}}$ is enthalpy at the intake and discharge state during isentropic process in kJ/kg, respectively.

3 Grid independence

In Table 3, comparison of the total solver CPU time and performance parameters between the fine, medium and coarse mesh density are presented. It can be seen from that the total solver CPU time increase with the cells number. The maximal deviation of the power output between the coarse and fine grids is about 9.88%, but the maximal deviation between the medium and fine grids is around 2.26%. Thus, the medium mesh density has relatively better accuracy precision and less solver time.

Table 3 Total solver CPU time and performance parameters under three different mesh density.

Case	Cells number (-)	Total solver time (h)	Power output (kW)	Deviation (%)
Coarse	1457276	186.68	3.023	9.88
Medium	2023860	223.46	2.812	2.26
Fine	3373369	340.52	2.751	-

4 Experimental verification

The experimental setup of SSE using compressed air is shown in Figure 6. The performance parameters can be obtained under different working conditions. The experimental cases at the intake pressure of about 0.7 MPa, intake temperature of 300K, and rotation speed of 3000rpm [12] are selected to validate the CFD model. Comparison between the simulation and experimental results at different working conditions are shown in Table 4. The relative deviation of mass flow rate and power output between the experimental and the simulation results are 7.92% and 8.92%. Thus, this CFD simulation can be used to analyze unsteady flow characteristics of SSE.

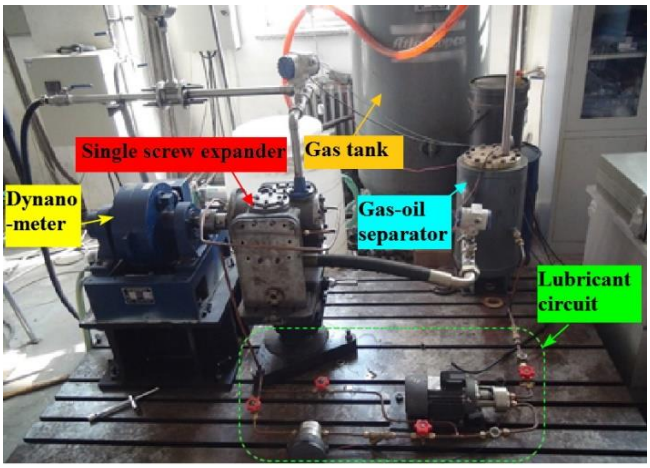

Figure 6 The experimental setup of SSE [12]

Table 4 Comparison between the simulation and experimental results

Prototype A	$\dot{m}$ (kg·s^{-1})	P (kW)
Simulation results	0.067	2.96
Experimental results	0.073	3.25
Relative error (%)	7.92	8.92

5 Results and discussion

5.1 Pressure field distribution

As a type of rotary positive displacement expander, periodicity is an inherent characteristic of SSE. There are six screw grooves in the SSE, the phase difference for each screw groove during one revolution is 360°/z1=60°. Six peaks can be identified during one revolution according to the phase difference of 60°. To study the unsteady flow in the SSE, the pressure, velocity and temperature field can directly reflect many kinds of transient information of in-cylinder flow. In order to observe the airflow state in the symmetrical working volume, the inclined section is given, as shown in Figure 5. Three different rotation angles (10º, 35º, 60º) have been given during one revolution.

The pressure field of rotors and working domain of inclined section are shown in Figure 7 and Figure 8, respectively. Once the screw groove volume communicated with the inlet triangle port, the high-pressure gas enters into the working volume formed by the screw groove, profile surfaces of the gaterotors teeth, and inside wall of the shell. The SG1(screw groove 1) with area of red color in a revolution is during the intake process. With the rotation of rotors, the high-pressure airflow cannot connect with the inlet port, the high-pressure airflow in the relatively close space begins expanding, SG2 at rotation angles of 35º and 60º, SG3 at rotation angles of 10º are during the expansion process, where is in orange and cyan color. After the expansion process, the low-pressure gas exhausts when the working volume communicated with the outlet port, the volume SG3 of blue color at rotation angles of 35º and 60º are during the discharge process. It also can be seen from Figure 8 that two symmetrical working chambers of left screw grooves (LSGs) and right screw grooves (RSGs) are accomplishing same process simultaneously and six screw grooves of screw rotor are exhausting throughout the whole working process.

Quantitative analysis of pressure in the screw groove is given in Figure 9, which shows the variation in pressure of adjacent three screw groove with screw rotor rotation angle based on the zero-dimensional thermodynamic chamber model. It indicates that the pressure of SG1 maintained at the 0.7MPa throughout one period, the pressure of SG2 is 0.7MPa, 0.6MPa and 0.36MPa and the pressure of SG3 is 0.3MPa, 0.22MPa and 0.18MPa at the screw rotor rotation angle of 10º, 35º and 60º, respectively. Thus, the pressure field distribution and pressure curve matched.

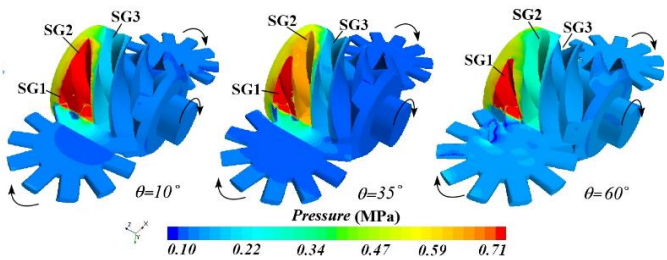

Figure 7 Pressure field distribution of rotors

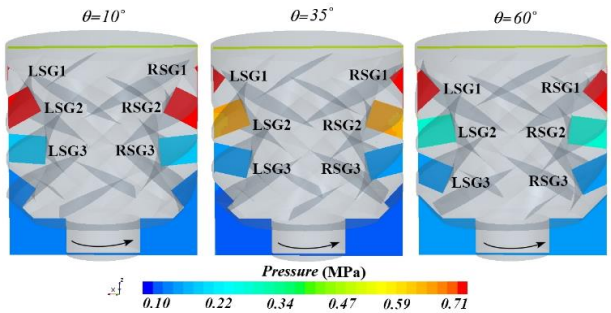

Figure 8 Pressure field distribution of working domain

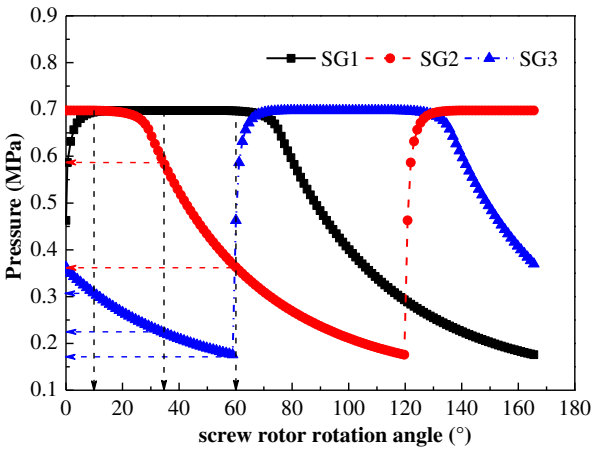

Figure 9 Variation in pressure of adjacent three screw groove with screw rotor rotation angle

5.2 Velocity field distribution

Figure 10 shows the velocity field distribution of the whole domain at three different rotation angles. As can be seen instantaneous velocity in the main flow region is less than sound velocity (<150 m/s) which indicates that unsteady flow in the SSE is subsonic flow. And the vortex motion of

airflow in the working chambers are different and vortex core changes with time in each chamber. The main reason for that is the mainstream flow in the working chamber changes with the rotation of the rotors. Besides, the disturbance of high-pressure airflow through the clearances have great influence on the vortex motion.

However, the instantaneous velocity near the meshing gap is higher than the sound velocity, attained up to 560 m/s, as is shown in Figure 11. The maximum of instantaneous velocity represented by red and yellow arrows are mainly distributed near the inlet region. The main reason for that is the high-pressure airflow at the inlet triangle hole will leak into the low-pressure adjacent working volume through the order of micrometer of meshing clearances.

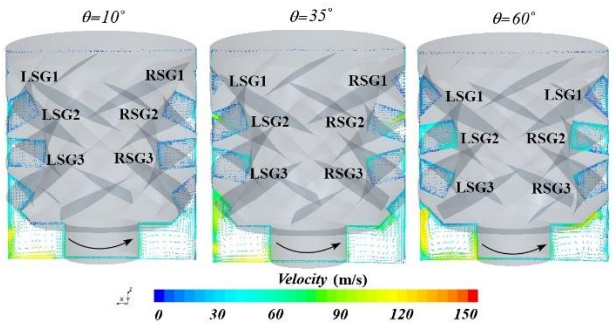

Figure 10 Velocity field distribution of the whole domain

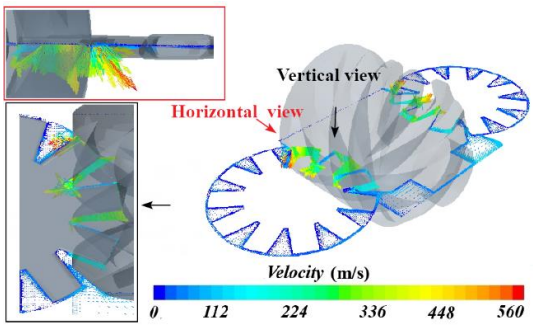

Figure 11 Velocity field distribution of meshing gaps

5.3 Temperature field distribution

The temperature field of rotors and working domain of inclined section at three different angles are shown in Figure 12 and Figure 13, respectively.

When the screw groove volume communicated with the inlet triangle port, this is during the intake process, the temperature of high-pressure gas is high, the high temperature value is about 300K, as shown in the red and orange area of SG1. When the high-pressure airflow expands during the expansion process, the temperature of gas will decrease with the rotation of rotors, the temperature values are in the range from 210K to 248 K, as shown in cyan and blue color. But the temperature will increase again in the discharge process, the temperature value is around 260K, as shown in green color. The main reason for that is the result of mixing of high temperature airflow and expanded low temperature airflow, because the high-temperature gas at the inlet triangle port leaks into outlet region through the gaterotors teeth surface gap.

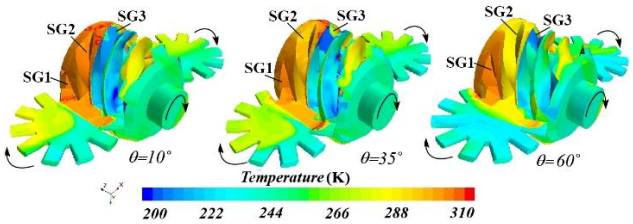

Figure 12 Temperature field distribution of rotors

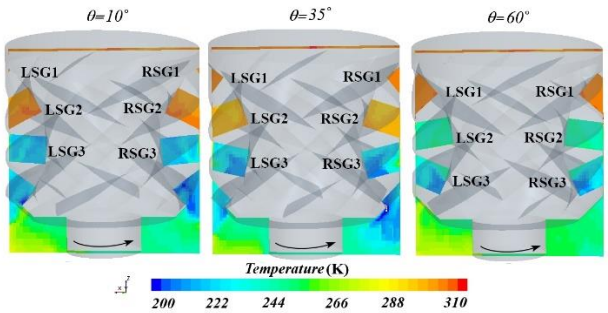

Figure 13 Temperature field distribution of working domain

Figure 14 shows the variation in temperature of adjacent three screw groove with screw rotor rotation angle based on the zero-dimensional thermodynamic chamber model. It indicates that the temperature of SG1 maintained at the 300K throughout one period, the pressure of SG2 is 300K, 295K and 248K and the temperature of SG3 is 230K, 204K and 188K at the screw rotor rotation angle of 10º, 35º and 60º, respectively.

5.4 Performance analysis

In order to analyze the energy loss under different volume ratio and rotation speed, a histogram of the column data is created. Figure 15 shows the energy loss caused by the viscous direct dissipation and turbulent dissipation, respectively. It indicates that the energy loss caused by the turbulent dissipation is the major energy loss, which is far larger than that of direct dissipation under different working conditions. Figure 16 shows the energy loss of three regions under different conditions. It can be seen from that the energy loss of middle domain is the largest, then the outlet region is the second most, and that of inlet region is the smallest.

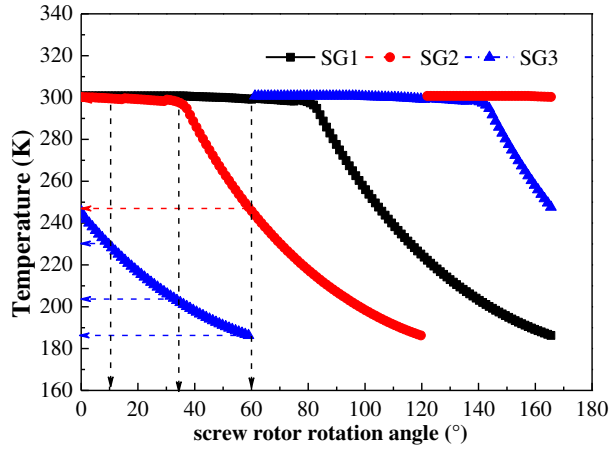

Figure 14 Variation in temperature of adjacent three screw groove with screw rotor rotation angle

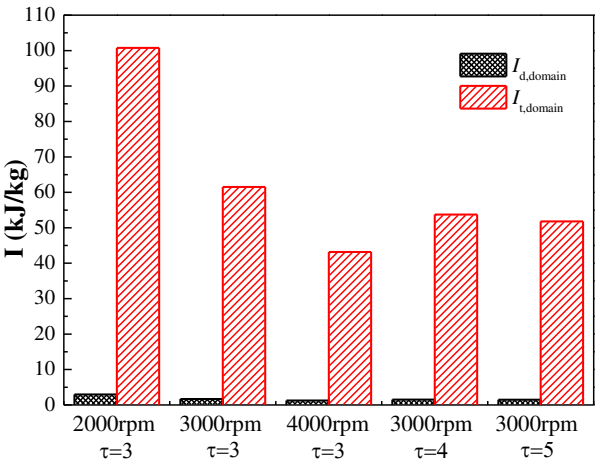

Figure 15 The energy loss caused by direct and turbulent fluctuation dissipation under different conditions

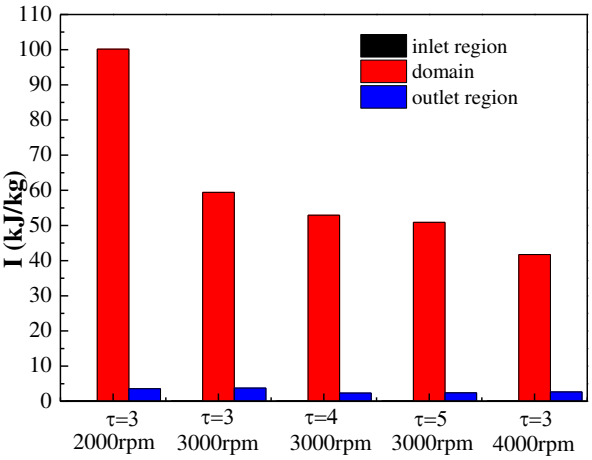

Figure 16 The energy loss of three regions under different conditions

The largest irreversible flow loss is at the middle domain including the screw rotor and gaterotors due to vortex motion of airflow at the spiral channel. Besides, Figure 15 and Figure 16 also show that the energy loss caused by irreversible flow loss decreases in the increase with the rotation speed and the internal volume ratio.

Variation of Energy loss factor and shaft efficiency under different rotation speed is shown in Figure 17. It can be seen from that the shaft efficiency first increases quickly then slowly with the increase in the rotation speed, while the energy loss factor first drops quickly then slowly with the rotation speed. The shaft efficiency increases from 37.4% to 40.5% and energy loss factor decreases from 0.547 to 0.221 when the rotation speed varies from 2000rpm to 4000rpm. It indicates that rotation speed has great effect on the energy loss and shaft efficiency of expanders. The main reason for that is the decrease in energy loss caused by irreversible flow loss when the rotation speed increases. In addition, less leakage at the higher rotation speed due to relatively less leakage time.

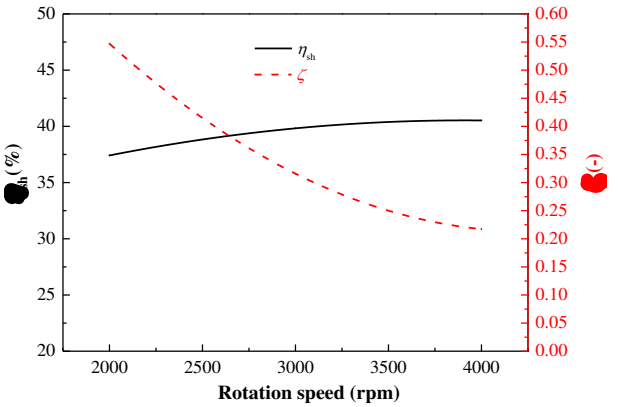

Figure 17 Variation of Energy loss factor and shaft efficiency under different rotation speed

The variation of energy loss factor and shaft efficiency under different internal volume ratio are shown in Figure 18. The shaft efficiency increases quickly then slowly with the increase in the internal volume ratio, the value changes from 39.8% to 52.1% when the internal volume ratio between 3 to 5. while the energy loss factor has little change and the value decreases from 31.6% to 30% with the internal volume ratio. This is because the smaller internal volume ratio, the larger intake triangle port and intake mass flow rate. The energy loss drops with the internal volume ratio when the working domain is same. Besides, the output power also decreases with the internal volume ratio. Both energy loss and output power play significant roles in shaft efficiency. Thus, shaft efficiency

increases in the increase of the internal volume ratio.

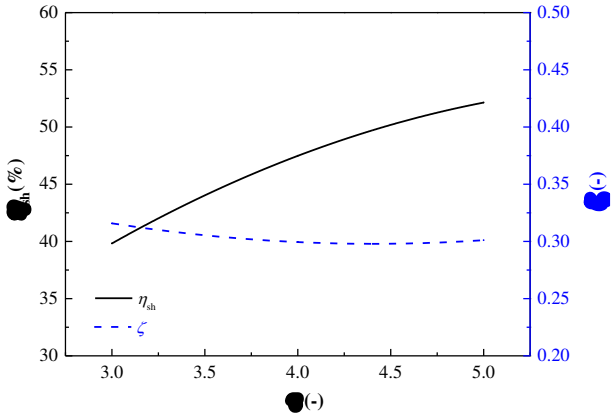

Figure 18 Variation of Energy loss factor and shaft efficiency under different internal volume ratio

6 Conclusions

(1). Two symmetrical working chambers in the SSE accomplish intake, expansion and discharge process at the same time. Six screw grooves of screw rotor are exhausting throughout the whole working process.

(2). The maximum of instantaneous velocity generated from the micrometer order meshing clearance is higher than the sound velocity due to the reduction of flow cross section. The instantaneous velocity of airflow in the mainstream workspace is less than sound velocity which indicates that unsteady flow in the SSE is subsonic flow.

(3). The energy loss of turbulent fluctuation dissipation is major loss, which if far larger than that of direct dissipation under different rotation speed and internal volume ratio. For the inlet, middle domain and outlet region, the energy loss of middle domain is the largest, the outlet region is the second most, and that of inlet region is the smallest.

(4). The energy loss factor decreases from 0.547 to 0.221 and shaft efficiency increases from 37.4% to 40.5% and when the rotation speed varies from 2000rpm to 4000rpm. The shaft efficiency increases with the increase in the internal volume ratio, the value changes from 39.8% to 52.1% when the internal volume ratio between 3 to 5.

Acknowledgements
The authors sincerely thanks to Professor Yu-ting WU of Beijing University of Technology for his critical discussion and reading during manuscript preparation.

Authors' Contributions
The author' contributions are as follows: LS and YW put forward the content of the paper; LS wrote the manuscript; WW and BL shared many theoretical knowledge and practical values. WD and RZ assisted in modifying the content and language expression of this paper.

Authors' Information
Lili Shen, born in 1991, is currently a PhD candidate at *Key Laboratory of Enhanced Heat Transfer and Energy Conservation, Ministry of Education and Key Laboratory of Heat Transfer and Energy Conversion, Beijing University of Technology, China*. She received her Ph.D from *Beijing University of Technology, China*, in 2020. Her research interests include theory and CFD simulation of single screw machines.

Yuting Wu, born in 1970, is currently a professor at *Key Laboratory of Enhanced Heat Transfer and Energy Conservation, Ministry of Education and Key Laboratory of Heat Transfer and Energy Conversion, Beijing University of Technology, China*.

Wei Wang, born in 1978, is currently an associate professor at *Key Laboratory of Enhanced Heat Transfer and Energy Conservation, Ministry of Education and Key Laboratory of Heat Transfer and Energy Conversion, Beijing University of Technology, China*.

Biao Lei, born in 1984, is currently an associate professor at *Key Laboratory of Enhanced Heat Transfer and Energy Conservation, Ministry of Education and Key Laboratory of Heat Transfer and Energy Conversion, Beijing University of Technology, China*.

Wei Duan, born in 1990, is currently an engineer at *Beijing Zhenxing Institute of Metrology and Measurement, China*.

Ruiping Zhi, born in 1986, is currently an instructor at *Key Laboratory of Enhanced Heat Transfer and Energy Conservation, Ministry of Education and Key Laboratory of Heat Transfer and Energy Conversion, Beijing University of Technology, China*.

Funding
Supported by National Key Research and Development Program of China (Grant No. 2017YFB0903603), National Natural Science Foundation of China (Grant No. 51706004).

Competing interests
The authors declare no competing financial interests.

Availability of data and materials
Not applicable

References

[1] M Imran, M Usman,B-S Park, et al. Volumetric expanders for low grade heat and waste heat recovery applications. *Renewable and Sustainable Energy Reviews*, 2016, 57: 1090-1109.

[2] J Li. Reversible single screw compressor/expander of energy storage and power generation system and methods. *China Patent* No. CN102352777A.

[3] D Ziniani, E A Groll, J E Braun. Review and update on the geometry modeling of single-screw machines with emphasis on expanders. *International Journal of Refrigeration*, 2018, 92: 10–26.

[4] Y Q Zhang, Y T Wu, G D Xia, et al. Development and experimental study on organic Rankine cycle system with single-screw expander for waste heat recovery from exhaust of diesel engine. Energy, 2014, 77: 499-508 .

[5] A Giuffrida. Improving the semi-empirical modelling of a single-screw expander for small organic Rankine cycles. *Applied Energy*, 2017, 193: 356-368.

[6] D Ziviani, S Gusev, S Lecompte, et al. Optimizing the performance of small-scale organic Rankine cycle that utilizes a single-screw expander. *Applied Energy*, 2017, 189: 416-32. .

[7] B Lei, W Wang, Y T Wu, et al . Development and experimental study on a single screw expander integrated into an Organic Rankine Cycle. *Energy*, 2016, 116: 43-52 .

[8] Y K Zhao, B Lei, Y T Wu, et al. Experimental study on the net efficiency of an Organic Rankine Cycle with single screw expander in different seasons. *Energy*, 165:769-775.

[9] W He, Y T Wu, Y H Peng, et al . Influence of Intake Pressure on the Performance of Single Screw Expander Working with Compressed Air. *Applied Thermal Engineering*, 2013, 51(2): 662-669 .

[10]W Wang, Y T Wu, C F Ma, et al. Experimental study on the performance of single screw expanders by gap adjustment. *Energy*, 2013, 62: 379-384.

[11] G Q Li, B Lei, Y T Wu, et al. Influence of inlet pressure and rotational speed on the performance of high pressure single screw expander prototype. *Energy*, 2018, 147: 279-285.

[12] W Wang, H Qiao, B Lei, et al. Experimental study on the influence of inlet and exhaust pressure loss on the performance of single screw expanders. *Energy*, 2021, 120912.

[13] V Lemort, S Quoilin, C Cuevas, et al. Testing and modeling a scroll expander integrated into an organic Rankine cycle. *Applied Thermal Engineering*, 2009, 29: 3094–102.

[14] E Winandy, S O Claudio, J Lebrun. Experimental analysis and simplified modeling of a hermetic scroll refrigeration compressor. *Applied Thermal Engineering*, 2002, 22(2):107-120.

[15] D Ziviani, S Gusev, S Lecompte, et al. Characterizing the performance of a single-screw expander in a small-scale organic Rankine cycle for waste heat recovery. *Applied Energy*, 2016, 181: 155-70.

[16] N Stosic, A Kovacevic, K Hanjalic, et al. Mathematical Modelling of the Oil Influence Upon the Working Cycle of Screw Compressors// *International Compressor Engineering Conference at Purdue*, West Lafayette, America, 1988: 354-361.

[17] H G Wu, Z W Xing, P C Shu. Theoretical and experimental study on indicator diagram of twin screw refrigeration compressor. *International journal of refrigeration*, 2004, 27(4):331-338.

[18]H G Wu, J Li, Z W Xing. Theoretical and experimental research on the working process of screw refrigeration compressor under superfeed condition. *International Journal of Refrigeration*, 2007, 30(8):1329-1335.

[19] X Zhang, Y Xu, J Xu, et al . Study on the performance and optimization of a scroll expander driven by compressed air. *Applied Energy*, 2017, 186:347-358.

[20] Z L Wang, Z B Wang, J Wang, et al. Theoretical and experimental study on thermodynamic performance of single screw refrigeration compressor with Multicolumn Envelope Meshing Pair. *Applied Thermal Engineering*, 2016, 103:139-149.

[21] L L Shen, W Wang, Y T Wu, et al. Theoretical and experimental analyses of the internal leakage in single-screw expanders. *International Journal of Refrigeration,* 2018, 76: 273-281.

[22] Y T Wu, Z Y Guo, B Lei, et al. Internal volume ratio optimization and performance analysis for single-screw expander in small-scale middle temperature ORC. *Energy*, 2019, 186: 115799.

[23] Z Y Guo, C C Zhang, Y T Wu, et al. Numerical optimization of intake and exhaust structure and experimental verification on single-screw expander for small-scale ORC applications. *Energy*, 199. 2020, 117478

[24] W Wang, L L Shen, R M Chen, et al. Numerical study of heat transfer influence on the performance of a single screw expander for Organic Rankine Cycle. *Energy*, 2020, 193: 119-130.

[25] A Suman, D Ziviani, J Gabrielloni. Different Numerical Approaches for the Analysis of a Single Screw Expander// *Conference of the Italian Thermal Machines Engineering Association*, 2016, 750–757.

[26] D Ziviani, A Suman, M Pinelli. CFD approaches applied to a single-screw expander// *23th International Compressor Engineering Conference at Purdue*, West Lafayette, America, 11-14 July, 2016.

[27] N Casari, A Suman, D Ziviani, et al. Computational models for the analysis of positive displacement machines: real gas and dynamic mesh. *Energy Procedia,* 2017, 129: 411-418.

[28] N Casari, E Fadiga, M Pinelli, et al. CFD Simulations of Single- and Twin-Screw Machines with OpenFOAM. *Designs* 2020, 4: 2.

[29] L L Shen, W Wang, Y T Wu, et al. Dynamic mesh technology for the simulation study of single screw expander. *Mechanisms and Machine Science,* 2020, 75: 885-889.

[30] N Casari, E Fadiga, M Pinelli, et al. Investigation of flow characteristics in a single screw expander: A numerical approach. *Energy*, 2020, 213: 118730.

[31] F Kock, H Herwig. Entropy production calculation for turbulent shear flows and their implementation in CFD codes. *International Journal of Heat and Fluid Flow*, 2005, 26(4): 672-680.

[32]H Herwig, F Kock. Direct and indirect methods of calculating entropy generation rates in turbulent convective heat transfer problems. *Heat and Mass Transfer*, 2007, 43(3): 207-215.

[33] F Kock, H Herwig. Local entropy production in turbulent shear flows: a high-Reynolds number model with wall functions. *International Journal of Heat & Mass Transfer,* 2004, 47(10/11): 2205-2215.